applied sciences

MDPI

Article

Study on the Difference in Wavefront Distortion on Beams Caused by Wavelength Differences in the Strong Turbulence Region

Meimiao Han [1], Xizheng Ke [1,2,*] and Jingyuan Liang [1]

[1] Faculty of Automation and Information Engineering, Xi'an University of Technology, Xi'an 710048, China; kambibiyo@163.com (M.H.); ljy@xaut.edu.cn (J.L.)
[2] Shaanxi Civil-Military Integration Key Laboratory of Intelligence Collaborative Networks, Xi'an 710126, China
* Correspondence: xzke@263.net

Abstract: In free-space optical communication, the transmission of signal light and beacon light of differing wavelengths through the same atmospheric channel encounters variations in how the atmospheric refractive index absorbs and scatters light. This leads to distinct degrees of wavefront aberrations between the signal and beacon lights. In this study, we employed statistical optics to derive wavefront phase structure functions for both signal and beacon lights under conditions of strong turbulence. We explored how wavefront distortion varies among beams of different wavelengths after propagation through such turbulent conditions. Our findings revealed that as the turbulence outer scale escalates, the difference in wavefront distortion between signal and beacon lights stabilizes after an initial increase, assuming constant wavelengths. Furthermore, we observed significant changes in the relative wavefront aberrations when the inner scale of turbulence surpasses the separation between two points on the receiving apertures. As the disparity in wavelength decreases, so does the difference in wavefront aberrations. Finally, we propose a method for correcting wavefront aberrations based on coefficients of Zernike polynomials corresponding to beams with different wavelengths. This approach is validated through simulation and experimentation, demonstrating an 11% enhancement in the signal-to-optical Strehl ratio and a 0.072 increase in spot energy after the addition of correction coefficients compared with before their inclusion. These results solidify the efficacy of our method in improving adaptive optics correction accuracy.

Keywords: adaptive optics; strong turbulence; wavefront distortion; wavefront-free correction; Zernike polynomials

Citation: Han, M.; Ke, X.; Liang, J. Study on the Difference in Wavefront Distortion on Beams Caused by Wavelength Differences in the Strong Turbulence Region. *Appl. Sci.* **2024**, *14*, 4692. https://doi.org/10.3390/app14114692

Academic Editor: Giampiero Contestabile

Received: 1 April 2024
Revised: 12 May 2024
Accepted: 27 May 2024
Published: 29 May 2024

1. Introduction

Atmospheric turbulence is typically classified by its intensity into strong turbulence, weak turbulence, and moderate turbulence. Strong turbulence refers to turbulence with high intensity accompanied by significant fluctuations. In regions of strong turbulence, a beam experiences significant phase and logarithmic amplitude fluctuations induced by atmospheric disturbances. The turbulent atmosphere fragments the beam's wavefront into numerous small speckles, creating a discontinuous phase surface marked by numerous phase singularities. This phenomenon leads to pronounced fluctuations in light intensity, causing flickering. During such conditions, the wavefront sensor struggles to accurately measure the complete distribution of the wavefront phase, resulting in a notable reduction in the efficacy of conjugate phase correction [1,2]. In contrast, wavefront sensor-less adaptive optics do not require a wavefront sensor to measure the distortion information of the signal light. Instead, it utilizes the control signal as an optimization parameter. Furthermore, parameters, such as imaging clarity, received optical energy, and other system performance indicators, can directly serve as objective functions for optimization algorithms. Leveraging

these algorithms can yield nearly optimal correction outcomes. Hence, this technology is suitable for rectifying wavefront aberrations in free-space laser communication systems operating amidst strong turbulence conditions [3,4]. In a free-space optical communication system, when the selected signal wavelength has poor penetration or severe attenuation in the atmospheric channel, the system employs beacon light with a wavelength different from signal light, in conjunction with the Acquisition, Pointing, and Tracking (APT) system, to achieve capture, aiming, and tracking, thereby establishing the communication link [5,6]. However, because of the different wavelengths of signal light and beacon light, atmospheric dispersion and beam diffraction effects may lead to differences in wavefront phase aberrations after atmospheric turbulence transmission [7,8]. When the correction system adjusts the signal light by measuring the beam quality of the beacon light emitted from the same optical path as the signal light, such as the Strehl Ratio (SR), an optimization parameter for wavefront correction algorithms, a divergence emerges between the beam SR value captured by the CCD camera, which measures the beacon light, and the actual SR value of the signal light. This discrepancy ultimately leads to a certain degree of residual aberration within the transmission even after the correction system has been applied.

In recent years, numerous studies have delved into the disparities in wavefront aberrations between signaling light and beacon light within dual-wavelength free-space optical communication systems. In 2007, Li discovered that the wavelength of a beam, alongside atmospheric turbulence and receiving aperture characteristics, influences the performance of adaptive optics systems [9]. Subsequently, in 2008, Nicholas identified variations in wavefront aberrations among different wavelengths transmitted through atmospheric turbulence, underscoring their significant impact on the correction of higher-order aberrations by adaptive optics systems [10]. In 2015, Gorelaya conducted an indoor space laser communication experimental link featuring the co-optical transmission of signal and beacon lights. Using a Shack–Hartmann wavefront sensor at the receiving end, Gorelaya measured the wavefront phase aberrations of optical signals at wavelengths of 530 nm and 1060 nm [11]. Additionally, in 2020, Xu scrutinized the polarization chromatic aberration between 1300 nm and 589 nm beams arising from the surface coating of the optical original in the Cassegrain optical antenna. The findings revealed that this type of polarization chromatic aberration encompasses out-of-focus aberration and a small amount of spherical aberration, with the out-of-focus aberration potentially reaching up to 1.14 rad [12]. Further contributing to the understanding of wavefront variances, Ke derived a formula for the overall undulation variance in the wavefront for beams of different wavelengths, highlighting differences in wavefront variance under identical transmission conditions [13]. Finally, in 2023, Wu discussed the wavefront distortion differences among beams induced by wavelength disparities in weak turbulence regions [14].

In general, wavefront aberration disparities in beams across weak turbulence, moderate turbulence, and strong turbulence regions are well-documented, albeit with less emphasis on the intricacies of the strong turbulence domain. Moreover, the challenge of effectively addressing aberration differences among beams of varying wavelengths in the strong turbulence region remains largely unresolved. In this article, we meticulously analyze the variances in wavefront phase aberrations within the received cross-section subsequent to the transmission of signal and beacon lights of disparate wavelengths through the strong turbulence region. Additionally, we propose a corrective coefficient method employing wavefront-free correction. This method relies on the relationships of Zernike polynomial coefficients corresponding to beams of different wavelengths. Ultimately, the efficacy of our proposed method is validated through simulation and experimentation.

2. Differential Analysis of Beam Wavefront Aberrations at Different Wavelengths in Regions of Strong Turbulence

Signal light with wavelength and beacon light with wavelength are Gaussian beams, which, after long-distance transmission through the atmospheric channel, arrive at the surface of the receiving antenna. This process can be approximated as plane wave incidence.

In the region of strong turbulence, the phase of the beam is torn into a discontinuous scattering distribution across the receiving cross-section. According to the Markov approximation, the following holds [15].

$$\langle n(R_1)n(R_2)\rangle = B_n(R_1 - R_2) = \delta(z)A(r_1 - r_2) \tag{1}$$

where $n(\cdot)$ denotes the refractive index of the air at a point on the cross-section of the transmission path, R_1 and R_2 represent any position vector on the transmission path cross-section, respectively, and B_n denotes the correlation function between different points. Furthermore, $A(r_1 - r_2)$ denotes the proportionality coefficient, where r_1 and r_2 represent the position vector on the receiving cross section, and its value in the strong turbulence region is tentatively set to 1 to guarantee uniform homogeneity. $\delta(z)$ is the shock response function that describes the response function to the effect of the turbulent phase, where z represents the transmission distance along the propagation path. The wavefront phase functions of the signal beam and the beacon beam at the receiving end can be approximated as response functions with phases modulated by turbulence. These can be expressed as follows [15]:

$$\phi_{\lambda_1} = k_1 \int_0^L \delta_n(\vec{r}, z)dz \tag{2}$$

$$\phi_{\lambda_2} = k_2 \int_0^L \delta_n(\vec{r}, z)dz \tag{3}$$

where ϕ_{λ_1} and ϕ_{λ_2} denoted the wavefront phase functions for wavelengths λ_1 and λ_2, respectively. L denotes the length of the transmission link, and $\mathbf{r}$ denotes the position vector in the receiver cross-section. Furthermore, $\delta_n(\vec{r}, z)$ denotes the shock response function; k_1 and k_2 denote the wave numbers corresponding to wavelengths λ_1 and λ_2, respectively. According to Equations (2) and (3), it is evident that the phase function response to atmospheric turbulence at a certain point on the receiving cross-section is related to the shock response function $\delta_n(\vec{r}, z)$ and the wave number $k = 2\pi/\lambda$. Therefore, the wavefront phase aberration of beams with different wavelengths after turbulence will differ. This dispersion non-equal halo error between the phases of beams of different wavelengths is represented by $\Delta\phi$ and can be expressed as:

$$\begin{aligned} \Delta\phi\left(\vec{r}\right) &= \phi_{\lambda_1} - \phi_{\lambda_2} \\ &= k_1 \textstyle\int_0^L \delta_n(\vec{r}, z)dz - k_2 \int_0^L \delta_n(\vec{r}, z)dz \end{aligned} \tag{4}$$

Based on Equation (4), it can be observed that $\Delta\phi$ is affected by the wavelength difference, transmission distance, distance between the two points in the received cross-section, and atmospheric turbulence. In regions of strong turbulence, the wavefront phase changes rapidly, which in turn leads to rapid and random changes in the aberration difference between the two wavefronts. These changes do not satisfy the conditions of a strictly smooth stochastic process [16]. The average value can only be maintained constant over a fairly short period. To solve this problem, instead of studying the difference value $\Delta\phi\left(\vec{r}\right)$ directly, we examine the rate of change in the difference value, denoted as $\Delta\phi\left(\vec{r}\right) - \Delta\phi\left(\vec{r}, \Delta t\right)$. We consider the relative rate of change to satisfy the conditions of a smooth stochastic process, and the values that change slowly can be described by the structure function $D_{\Delta\phi}\left(\vec{\rho}\right)$ of the phase difference as follows:

$$D_{\Delta\phi}\left(\vec{\rho}\right) = \left\langle \left[\Delta\phi\left(\vec{\rho} + \vec{r}\right) - \Delta\phi\left(\vec{r}\right)\right]^2 \right\rangle \tag{5}$$

where $\vec{\rho}$ denotes the position vector between two points on the receiving cross-section and $\langle\cdot\rangle$ represents ensemble average. From Equation (5), it can be observed that the total

amount of the phase structure function is composed of a stabilizing quantity and small portion that exhibits slight variations. The spatial distribution of these variations in the receiving cross-section can be expressed as follows:

$$\begin{aligned} D_{\Delta\phi}\left(\vec{\rho}\right) &= \left\langle \left[\Delta\phi\left(\vec{\rho}+\vec{r}\right)-\Delta\phi\left(\vec{r}\right)\right]^2 \right\rangle \\ &= 2\left[B_n\left(\vec{\rho}\right)-B_n\left(\vec{r}\right)\right] \end{aligned} \tag{6}$$

where B_n denotes the mutual coherence function. The phase response function is defined as the response to a unit impulse that is uniformly distributed across the receiving surface. At this point, the impact of atmospheric turbulence on the optical phase front can be described by the distribution of refractive index variations, which establishes a relationship between the structure function of phase difference and structure function for the random distribution of refractive index. This relationship is denoted as follows:

$$\begin{aligned} D_{\Delta\phi}\left(\vec{r}\right) &= \left\langle \left[\left(k_1\int_0^L \delta_n\left(\vec{r}_1,z\right)dz\right)-\left(k_2\int_0^L \delta_n\left(\vec{r}_2,z\right)dz\right)\right]^2 \right\rangle \\ &= (k_1-k_2)^2\left\langle \left[\left(\int_0^L \delta_n\left(\vec{r}_1,z\right)dz\right)-\left(\int_0^L \delta_n\left(\vec{r}_2,z\right)dz\right)\right]^2 \right\rangle \\ &= (k_1-k_2)^2 D_n\left(\vec{r}\right) \end{aligned} \tag{7}$$

where $D_n\left(\vec{r}\right)$ denotes the phase structure function of atmospheric turbulence. Based on the relationship between the turbulent power spectrum and phase structure function, the following relationship for $D_n\left(\vec{r}\right)$ can be obtained [17] as follows:

$$\begin{aligned} D_n\left(\vec{\rho}\right) &= 2\left[B_n\left(\vec{r}+\vec{\rho}\right)-B_n\left(\vec{r}\right)\right] \\ &= 8\pi\int_0^\infty \kappa^2\Phi(\kappa)\left[1-\frac{\sin(k\rho)}{k\rho}\right]d\kappa \end{aligned} \tag{8}$$

where $B_n\left(\vec{r}\right)$ represents the number of interrelationships between two points on the spot, κ denotes the number of spatial waves, and $\Phi(\kappa)$ denotes the spatial power spectrum of the turbulence. The modified von-Kármán power spectrum is used here, and it can be expressed as:

$$\Phi(\kappa) = 0.033C_n^2\frac{\exp\left(-\kappa^2/\kappa_m^2\right)}{\left(\kappa^2+\kappa_0^2\right)^{11/6}}, 0 \le \kappa < \infty \tag{9}$$

In the above equation, the relationship between the parameter κ_0^2 and outer scale L_0 of turbulence can be expressed as $\kappa_0 = c_0/L_0$, where c_0 denotes a proportionality parameter. Typically, its value is 8π in the region of strong turbulence. Furthermore, C_n^2 denotes the atmospheric refractive index structure constant, which characterizes the strength of the turbulence and is a constant in horizontal transport. When $C_n^2 < 10^{-17}$ m$^{-2/3}$, turbulence intensity is weak; $C_n^2 > 10^{-13}$ m$^{-2/3}$ indicates strong turbulence intensity; and 10^{-17} m$^{-2/3}$ $< C_n^2 < 10^{-13}$ m$^{-2/3}$ corresponds to moderate turbulence intensity [17]. κ_m denotes a parameter that is related to l_0 and can be expressed as $\kappa_m = 5.92/l_0$, where l_0 denotes the internal scale of turbulence. The expansion $\left[1-\frac{\sin(\kappa\rho)}{\kappa\rho}\right]$ in Equation (8) can be expressed using the Maclaurin series as [17]:

$$\left[1-\frac{\sin(\kappa\rho)}{\kappa\rho}\right] = \sum_{n=1}^{\infty}\frac{(-1)^{n-1}}{(2n+1)!}(\kappa\rho)^{2n} \tag{10}$$

By substituting Equations (9) and (10) into Equation (8) and integrating, Equation (8) becomes [17]:

$$\begin{aligned} D_n\left(\vec{\rho}\right) &= 1.685C_n^2\kappa_m^{-2/3}\left[{}_1F_1\left(-\tfrac{1}{3};\tfrac{3}{2};-\tfrac{\kappa_m^2\rho^2}{4}\right)-1\right] \\ &+1.050C_n^2\kappa_0^{-2/3}\left[1-{}_0F_1\left(-;\tfrac{2}{3};-\tfrac{\kappa_0^2\rho^2}{4}\right)\right], \kappa_0 \ll \kappa_m \end{aligned} \tag{11}$$

By substituting Equation (11) into Equation (7) and transforming, Equation (7) can be expressed as:

$$\begin{aligned} D_{\Delta\phi}\left(\vec{r}\right) &= 1.685C_n^2(k_1-k_2)^2\kappa_m^{-2/3}\left[{}_1F_1\left(-\tfrac{1}{3};\tfrac{3}{2};-\tfrac{\kappa_m^2\rho^2}{4}\right)-1\right] \\ &+1.050C_n^2(k_1-k_2)^2\kappa_0^{-2/3}\left[1-{}_1F_1\left(1;\tfrac{2}{3};\tfrac{\kappa_0^2\rho^2}{4}\right)\right], \kappa_0 \ll \kappa_m \end{aligned} \tag{12}$$

where function ${}_1F_1(a;c;x)$ is a type of confluent hypergeometric function. It can serve as an approximation for large parameters when the distance ρ between two points on the receiver's cross-section satisfies the condition $l_0 \ll \rho \ll L_0$. This approximation for large parameters is provided in [17]:

$${}_1F_1(a;c;-x) \sim \frac{\Gamma(c)}{\Gamma(c-a)}x^{-a} \tag{13}$$

where $\Gamma(\cdot)$ denotes the gamma function.

When distance ρ between two points on the receiving cross-section satisfies the condition of $\rho \ll l_0$. The following small parameter approximation can be used [17]

$${}_1F_1(a;c;-x) \sim 1-\frac{a}{c}x \tag{14}$$

When the above-mentioned equation is combined with Equation (12), it can be observed that the beam wavefront aberration difference is not only related to the beam wavelength but also closely related to the inner and outer turbulence scales.

The wavefront sensor fails to capture the continuous phase distribution within the strong turbulence region, rendering the phase relationship unusable for correcting wavefront aberrations. Additionally, conventional geometric optics analysis proves insufficient for analyzing wavefront phase across different wavelengths. Consequently, we opted for the statistical optics method, also termed as the phase structure function method. In statistical optics, the coefficient average, also referred to as the ensemble average, can be considered equal to the time average of a single stochastic process under the preconditions of a generalized stochastic smooth process. Leveraging the definitions of the coefficient average and root mean square (RMS), we derive the RMS of the error between beams of varying wavelengths by squaring the mean square value of Equation (12), which can be expressed as:

$$\mathrm{RMS} = \sqrt{D_{\Delta\phi}\left(\vec{r}\right)} \tag{15}$$

It is assumed that the values of the outer scale of turbulence L_0 correspond to 20 m, 30 m, 50 m, 60 m, or 80 m, the turbulence inner scale parameter l_0 is 0.1 m, and the atmospheric refractive index structural parameter value is $C_n^2 = 1 \times 10^{-12}$ m$^{-2/3}$. When signal light with a wavelength of 1550 nm and beacon light with a wavelength of 632.8 nm are transmitted in the atmospheric channel in a co-optical path with L = 10 km, the variation curves of the difference RMS in the wavefront phase aberration between different points on the received cross-section are shown in Figure 1. Figure 1 illustrates the beam wavefront aberration difference at the receiving end cross-section with the augmentation of the outer scale of turbulence when the distance between the two points is held constant. Notably, beyond an outer scale of 40 m, the rate of change in wavefront aberration diminishes, suggesting a gradual reduction in the impact of the turbulence outer scale on beam modu-

lation. Furthermore, when the outer scale of turbulence is fixed, an increase in the distance between the two points at the receiver does lead to a higher wavefront aberration at the receiver's cross-section; however, this overall variation magnitude remains relatively small. This observation underscores that, while different distances between two points influence the wavefront aberration at the receiver's cross-section to some extent, the effect is not substantial.

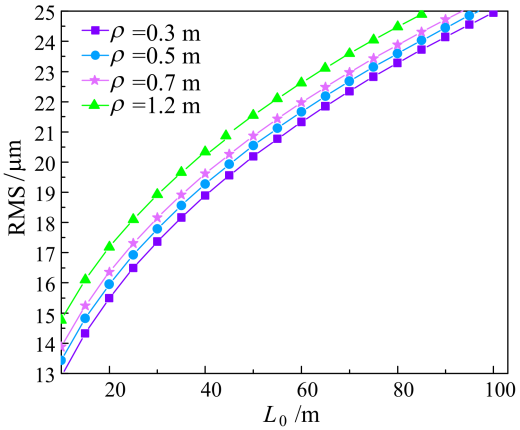

Figure 1. The influence of the distance between two points on the wavefront phase aberration difference for beams with different wavelengths.

It is assumed that the turbulence inner scale l_0 values range from 0.01 m to 0.15 m and from 0.2 m to 0.4 m, with a turbulence outer scale parameter of L_0 = 40 m and an atmospheric refractive index structural constant value of $C_n^2 = 1 \times 10^{-12}$ m$^{-2/3}$. When signal light with a wavelength of 1550 nm and beacon light with a wavelength of 632.8 nm are transmitted through the atmospheric channel on a co-optical path with L = 10 km, the influence of the turbulence inner scale on the RMS difference in wavefront phase aberration across various points on the received cross-section is shown in Figure 2. Upon comparing Figure 2a,b, it becomes apparent that when the separation between the two points is smaller than the inner scale of turbulence, there is a discernible effect on the wavefront phase aberration difference. As the distance between the points increases and approaches the inner scale of turbulence, this effect gradually diminishes, and the curves begin to overlap significantly. Subsequently, when the distance between the points surpasses the inner scale of turbulence, the wavefront phase aberration differences stabilize and the curves' slopes exhibit no significant changes. This outcome may be attributed to beam diffraction within small-scale turbulence. However, as the distance between the points extends beyond the inner scale of turbulence, the light undergoes refraction once more, leading to a diminished influence of small-scale turbulence on the beam.

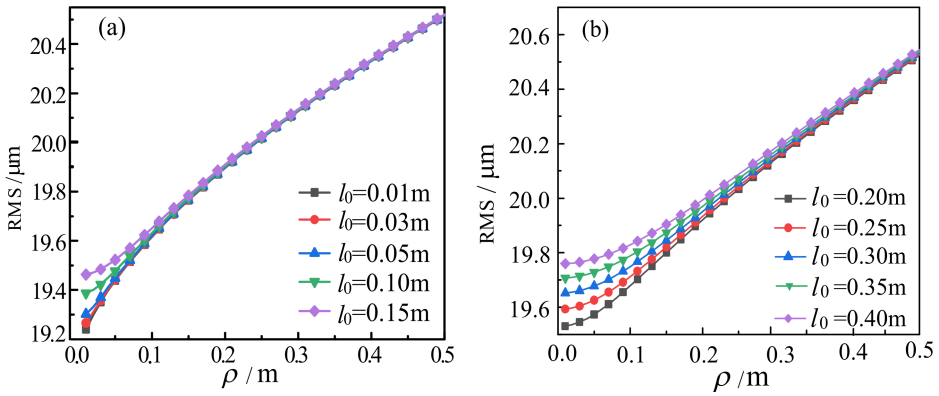

Figure 2. Influence of the turbulence inner scale on the difference in wavefront aberrations of beams with different wavelengths: (**a**) l_0 = 0.01 m ~ l_0 = 0.15 m and (**b**) l_0 = 0.20 m ~ l_0 = 0.40 m.

It is assumed that the turbulence inner scale l_0 is 0.10 m, turbulence outer scale L_0 is 50 m, and atmospheric refractive index structure constant corresponds to $C_n^2 = 1 \times 10^{-12}$ m$^{-2/3}$. Signal light with a wavelength of 1550 nm and beacon lights with wavelengths of 632.8 nm, 530 nm, 850 nm, and 950 nm traverse the atmospheric channel along a shared optical path spanning 10 km. Variations in wavefront phase aberration across different points on the received cross-section are influenced by these wavelength discrepancies, as depicted in Figure 3. In Figure 3a, within the receiving aperture cross-section, the distance between two points exhibits minimal impact on the wavefront aberration difference between beams of distinct wavelengths, consistently maintaining a stable level. Notably, when the beacon light wavelength is 1280 nm, the disparity between the signal light and beacon light wavefront aberration remains below 1, rendering it practically negligible. Figure 3b highlights that as the wavelength disparity between the signal light and the beacon light diminishes, the wavefront aberration difference progressively decreases. When the wavelengths of the signal light and the beacon light align, the wavefront aberration difference reaches 0. Thus, only when the signal light and beacon light wavelengths closely match, the accuracy of adaptive optics for wavefront correction can be maximized. Consequently, in practical applications, the wavelength difference between beacon light and signal light should be considered a critical factor when selecting the beacon light wavelength.

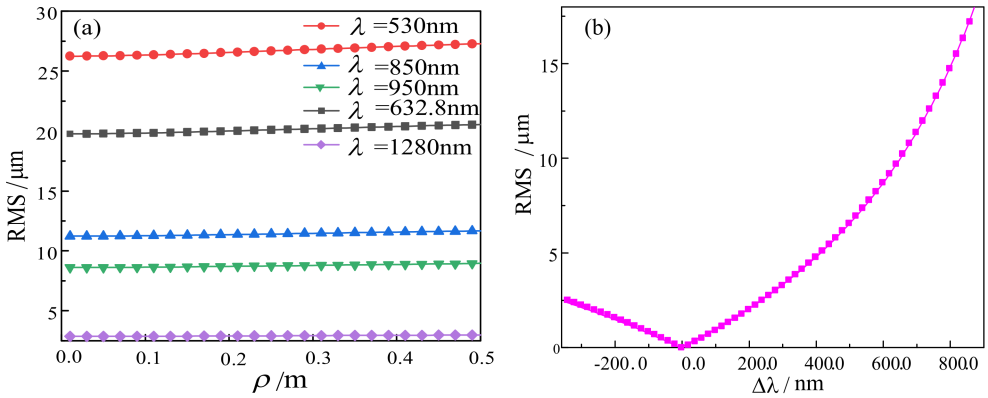

Figure 3. The difference in beam wavefront phase distortion between different points on the receiving cross-section. (**a**) Different wavelengths. (**b**) Difference between different wavelengths.

3. Signal Optical Wavefront Aberration Correction for Dual-Wavelength Free-Space Optical Communication Systems

3.1. Theory

Zernike polynomials are a set of mutually orthogonal polynomials defined within a unit circle. Their coefficients, which are linear combinations of basis functions, can accurately describe different types of wavefront aberrations. Wavefront aberration, $\phi(\rho, \theta)$, can be expressed as a linear combination of Zernike polynomials [17]:

$$\phi(\rho) = \sum_{i=1}^{N} a_i z_i(\rho, \theta) \tag{16}$$

where N denotes the total aberration order, a_i denotes the coefficient of the Zernike polynomial of order i, (ρ, θ) denotes the polar coordinate, and $Z_i(\rho, \theta)$ denotes the expression of the Zernike polynomial of order i in polar coordinates as follows:

$$Z_i = \begin{cases} \sqrt{n+1} R_n^m(\rho) \sqrt{2} \cos(m\theta) & m \neq 0 \text{ and } m \textit{ is even} \\ \sqrt{n+1} R_n^m(\rho) \sqrt{2} \sin(m\theta) & m \neq 0 \text{ and } m \textit{ is odd} \\ \sqrt{n+1} R_n^m(\rho) & m = 0 \end{cases} \tag{17}$$

where

$$R_n^m(\rho) = \sum_{s=0}^{\frac{n-m}{2}} \frac{(-1)^s (n-s)!}{s![(n+m/2)-s]![(n-m/2)-s]!} \rho^{n-2s} \tag{18}$$

where m and n denote the angular and radial numbers in polar coordinates of the Zernike polynomials, respectively. The essence of employing Zernike polynomials to model wavefront aberrations lies in determining both the order of the polynomials and the coefficients associated with each order. Essentially, higher-order Zernike polynomials encompass a broader spectrum of aberrations, thereby yielding greater fitting accuracy. Following the fitting of Zernike polynomials to the wavefront aberration phase for signal and beacon lights of varying wavelengths, discrepancies emerge in the coefficient matrices of the Zernike polynomials corresponding to the two beams within the same Zernike mode order.

The coefficients of the Zernike polynomials, which represent wavefront aberrations for signal light at wavelength λ_1 and for beacon light at wavelength λ_2, can be expressed as follows [17]:

$$\begin{array}{l} a_1(\lambda_1), a_2(\lambda_1), a_3(\lambda_1), \ldots\ldots, a_j(\lambda_1) \\ a_1(\lambda_2), a_2(\lambda_2), a_3(\lambda_2), \ldots\ldots, a_j(\lambda_2) \end{array} \tag{19}$$

The numerical relationship between the coefficients of Zernike polynomials of the same order can be established through the wavelength function, which can be expressed as:

$$\begin{array}{l} a_1(\lambda_1) = f_1[a_1(\lambda_2), \lambda_1] \\ a_2(\lambda_1) = f_2[a_2(\lambda_2), \lambda_1] \\ \quad \vdots \\ a_j(\lambda_1) = f_j[a_j(\lambda_2), \lambda_1] \end{array} \tag{20}$$

Based on the actual transmission process of laser communication, we established a mode analysis model to determine the functional relationship among polynomial coefficients. We selected an infinitesimal region, denoted as $\Delta\delta$, on the wavefront phase plane and directed the signal light and beacon light into a common optical path. Assuming perfect alignment, the corresponding region $\Delta\delta$ experiences the same transmission path through the atmospheric channel and the same variations in refractive index. Based on "Taylor's" frozen-flow hypothesis [18], we selected a particular instant as the time for analysis. At this moment, the combined fluctuations in the atmospheric refractive index along the path of the beam can be approximated by a lens with an inhomogeneous refractive index distribution. This approximation can be analyzed using the formula for refractive index dispersion, which is commonly used for engineering materials. The relationship between the coefficients of the Zernike polynomials and wavelength can be expressed as follows [19]:

$$a_i = A_i + \frac{B_i}{\lambda} + \frac{C_i}{\lambda^{3.5}} \tag{21}$$

where a_i denotes the coefficient of the Zernike polynomial of order i, and A_i, B_i, and C_i denote the coefficients of the Conrady–Zernike polynomial. When the wavelengths differ, the relationship between their corresponding coefficients can be expressed as follows:

$$a_i(\lambda_1) = \left[\left(A_i + \frac{B_i}{\lambda_1} + \frac{C_i}{\lambda_1^{3.5}} \right) / \left(A_i + \frac{B_i}{\lambda_2} + \frac{C_i}{\lambda_2^{3.5}} \right) \right] a_i(\lambda_2) \tag{22}$$

The proportionality correction factor between the ith order Zernike polynomial coefficients corresponding to the signal light and beacon light is as follows:

$$Z_i = \left[(A_i + \frac{B_i}{\lambda_1} + \frac{C_i}{\lambda_1^{3.5}}) / (A_i + \frac{B_i}{\lambda_2} + \frac{C_i}{\lambda_2^{3.5}}) \right] \tag{23}$$

Considering the 15th-order Zernike polynomial as an example, the Zernike polynomial coefficient vector corresponding to beacon light can be expressed as:

$$\mathbf{A}_{15}(\lambda_2) = [a_1, a_2, a_3, \cdots, a_{15}]^{\mathrm{T}} \tag{24}$$

After multiplying the coefficient vector of the beacon light with the corresponding correction vector, we obtain:

$$\begin{aligned} \mathbf{A}^{'}{}_{15}(\lambda_2) &= \begin{bmatrix} z_1, 0, 0, \ldots, 0 \\ 0, z_2, 0, \ldots, 0 \\ \vdots \\ 0, 0, 0, \ldots, z_{15} \end{bmatrix} [a_1, a_2, a_3, \cdots, a_{15}]^{\mathrm{T}} \\ &= [z_1 a_1, z_2 a_2, z_3 a_3, \cdots, z_{15} a_{15}]^{\mathrm{T}} \end{aligned} \tag{25}$$

Furthermore, the mutual covariance matrix of the modified polynomial coefficients can be expressed as [20]:

$$\begin{aligned} \mathbf{C}^{'} &= E\left[A'_{15}(\lambda_2) \cdot A'^{\mathrm{T}}_{15}(\lambda_2)\right] \\ &= \begin{bmatrix} E(z_1a_1, z_1a_1) & E(z_1a_1, z_2a_2) & \cdots & E(z_1a_1, z_Na_N) \\ E(z_2a_2, z_1a_1) & E(z_2a_2, z_2a_2) & \cdots & E(z_2a_2, z_Na_N) \\ \vdots & \vdots & \ddots & \vdots \\ E(z_Na_N, z_1a_1) & E(z_Na_N, z_2a_2) & \cdots & E(z_Na_N, z_Na_N) \end{bmatrix} \end{aligned} \tag{26}$$

The covariance matrix $\mathbf{C}^{'}$ is known as a Hermitian matrix [20]. Hence, there exists a unitary matrix $\mathbf{X}$ such that it is a diagonal array. We perform singular value decomposition of the covariance matrix $\mathbf{C}^{'}$ as follows:

$$\mathbf{C}^{'} = \mathbf{X}\mathbf{S}\mathbf{X}^{\mathrm{T}} \tag{27}$$

It is assumed that the coefficient vector of another linear combination B of wavefront Zernike polynomials of the same dimension as A is $\mathbf{B} = [b_1, b_2, \ldots, b_N]^{\mathrm{T}}$. Then, the Zernike polynomial coefficients of the wavefront of the corresponding signal optical distortion are:

$$\mathbf{A}^{'} = \mathbf{X} \cdot \mathbf{B} \tag{28}$$

3.2. Simulation Verification

The wavefront correction system uses a charge-coupled device (CCD) camera to measure the spot energy, Strehl ratio, and other beam parameters of the laser beam, which are used as optimization indicators for the control program and converted into control signals for the deformable mirror [20,21]. The working principle of the system is shown in Figure 4, which mainly includes the following three parts: wavefront controller, wavefront corrector (deformable mirror, DM), and imaging detector (CCD). The parallel light generated by the light source forms distorted beams carrying aberrations after undergoing atmospheric turbulence transmission. This distorted beam is projected onto the deformable mirror, which corrects the distortion for the first time and reflects the remaining distorted beam onto the CCD. Next, the wavefront controller drives the intelligent algorithm to recalculate the control instructions of the deformable mirror based on the system performance indicators collected by the CCD. The deformable mirror corrects the wavefront distortion of the beacon light by adjusting its surface morphology. This process is cyclic, and after each round of correction, the deformable mirror further adjusts its shape based on the newly obtained feedback information of the light spot, gradually approaching the ideal correction state and achieving multiple closed-loop corrections of the distorted beam.

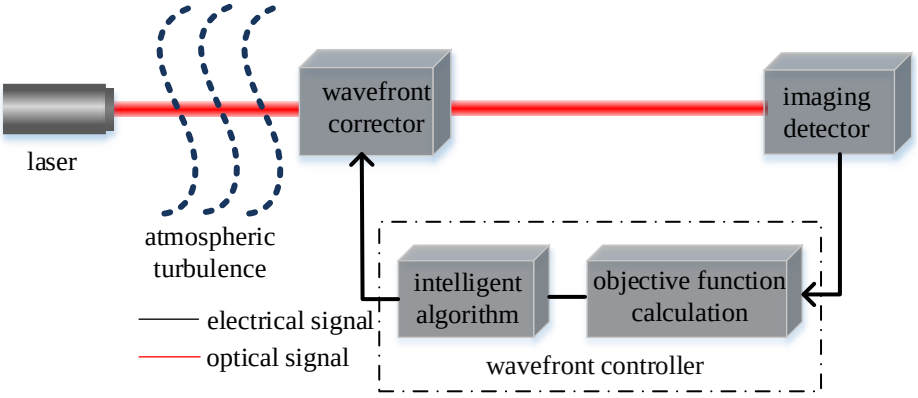

Figure 4. The working principle of the wavefront correction system.

The control system adopts the stochastic parallel gradient descent (SPGD) algorithm. The algorithm first generates the basic voltage command for the deformable mirror and superimposes a random perturbation voltage signal that conforms to the Bernoulli distribution. On this basic voltage, forward and reverse voltage disturbances are applied separately, and then the change in the system objective function under each disturbance voltage is calculated. Finally, based on the calculation principles shown in Figure 5, the voltage signal that should be applied during the iteration cycle is determined. This process continues to loop until the system objective function reaches the preset optimization conditions.

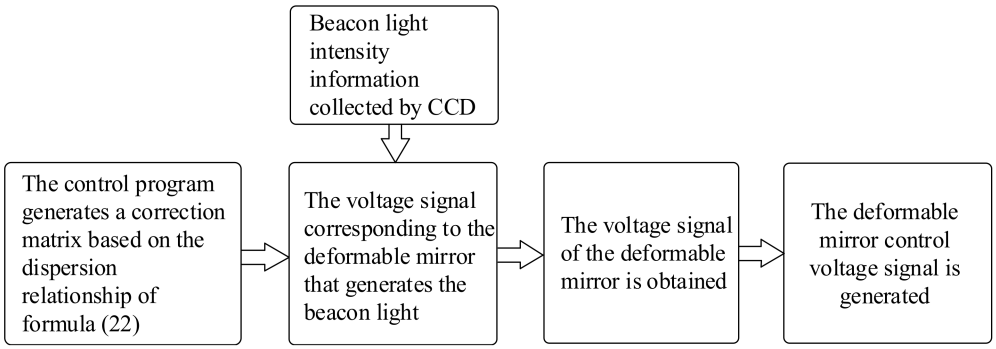

Figure 5. Schematic diagram of the correction of wavefront aberration differences without wavefront correction.

In conditions characterized by an atmospheric coherence length $r_0 = 0.01$ m, a disturbance amplitude $\delta = 0.006$, a high gain coefficient of $\gamma = 1.6/(1 + J)$ (where J denotes the value of the system's objective function), and 100 iterations, numerical simulations were conducted to investigate the performance of dual-wavelength wavefront-free sensing adaptive optics technology in correcting far-field spot SR under atmospheric turbulence. The simulations employed the multi-phase screen method to model laser beam propagation through a turbulent atmosphere, with phase screens generated using Zernike polynomials [22]. The specific parameters for the simulation included a signal wavelength of 1550 nm, a beacon wavelength of 632.8 nm, a transmission distance of 10 km, a phase screen interval of $\Delta z = 1500$ m, and a phase screen size of D = 0.4 m. The Zernike coefficient matrices for the beacon light, both pre- and post-correction, were integrated into the adaptive optics control system to rectify the wavefront aberration of the signal light. The resulting changes in SR for the signal light are depicted in Figure 6. Analysis of the figure reveals that over 100 iterations of correction, the SR value of the signal beam within the correction system lacking additional correction coefficients exhibits slow convergence, reaching a limit of 0.89, accompanied by notable jitter during the correction process. Conversely, the system augmented with correction coefficients realizes a higher SR value limit of 0.982, marking

an 11% enhancement over the initial convergence target of 0.89. Furthermore, it attains convergence more rapidly, stabilizing at 70 iterations with significantly reduced jitter.

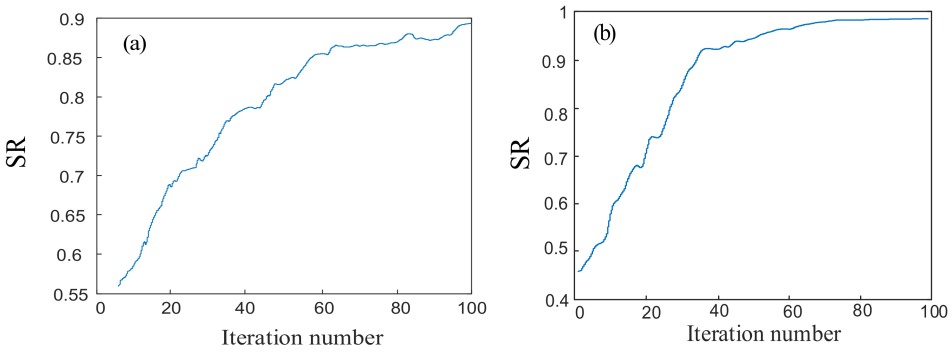

Figure 6. Signal light SR value variation curve with the number of iterations. (**a**) Without the wavefront correction coefficient. (**b**) With the wavefront correction coefficient.

3.3. Experimental Research

The wavefront-free adaptive optics correction system is constructed indoors, with the experimental design principle illustrated in Figure 7. Both the signal light and the beacon light, emanating from a shared optical path, traverse through polarizer P1 before entering a 4F system comprising lenses L1 and L2 for beam expansion and collimation. Subsequently, the collimated beam proceeds to a spatial light modulator after being split by beam splitter BS1. Loaded with a phase screen, the spatial light modulator modulates the collimated light, and the modulated beam is reflected by mirror PM. Following reflection, the beam is again divided by BS2 and directed to the deformable mirror (DM). Here, the DM undertakes the initial correction of the distorted light, which is then converged through lens L3 and directed to the CCD. Furthermore, the CCD captures the intensity of the distorted beam and transmits this information to the computer. Utilizing optimization algorithms, the computer generates control signals for the deformable mirror, thereby executing multiple closed-loop corrections of the wavefront aberrations. The detailed equipment parameters employed in the experiment are outlined in Table 1.

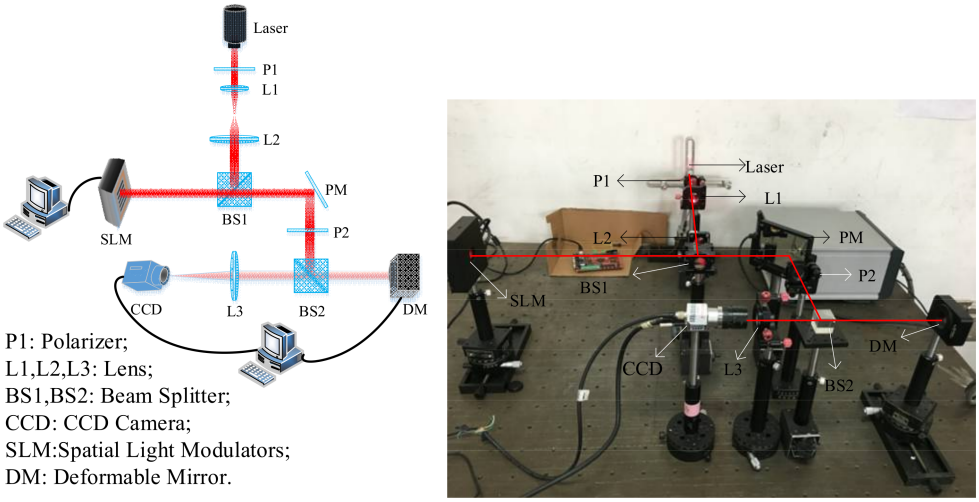

Figure 7. Experimental schematic diagram of wavefront sensor-less adaptive optics.

Table 1. Parameters of experimental equipment.

Equipment Name	Type	Equipment Parameter
Liquid crystal spatial light modulator	RL-SLM-R2	Target size: 0.78″ Pixel size: 12.3 mm Operating wavelength: 400~1620 nm Phase modulation capability: 0~2π@532 nm
Deformable mirror	ALPAO-DM	Number of actuators: 69 Pupil diameter: 10.5 mm Oblique wavefront modulation: 60 mm Bandwidth: >750 Hz Setting time: 800 µs Analog response time: <10 µs
CCD	MW-GX-650	Pixel Size: 5.5 mm × 5.5 mm Frame rate: 8 fps Exposure time: 300–1,000,000 ms

In the experiments, we selected wavelengths of 1550 nm as the signal light and 632.8 nm as the beacon light, respectively. The turbulent phase screen based on the Zernike polynomial method was loaded into the liquid crystal spatial light modulator (LC-LSM) to cause wavefront distortion of the beam [23–25]. The SPGD algorithm based on the variable gain coefficient was used to correct the wavefront distortion. We used the average grey scale value of 10 × 10 pixel area centered on the spot's center of mass, as captured by the CCD camera, to evaluate the calibration effect in terms of spot brightness. The size of the phase screen was D = 0.4 m. For the SPGD algorithm, we selected a perturbation amplitude value of $\delta = 0.006$ and a gain coefficient value of $\gamma = 1.6/(1 + J)$. In order to simulate strong turbulence conditions, we set the atmospheric coherence length to r_0 = 0.01 m [26,27]. We conducted closed-loop correction experiments, and the results are shown in Figure 8a,b. By comparing the two figures, we can observe that the system without wavefront correction has a significant correction effect on the wavefront aberration in regions of strong turbulence. The SR value of the spot prior to correction stands at 0.112. Post-correction, it notably increases to 0.74, signifying a substantial enhancement in spot energy convergence. Upon employing the SPGD algorithm to generate the adaptive mirror voltage control signal, correction coefficients are incorporated to address the aberrations of the signal light. As depicted in Figure 8c, the results illustrate heightened spot energy compared with Figure 8b, where the dark spot is rectified. Notably, the beam's SR value escalates to 0.812, underscoring the effectiveness of this approach in further refining the system's correction accuracy without wavefront correction.

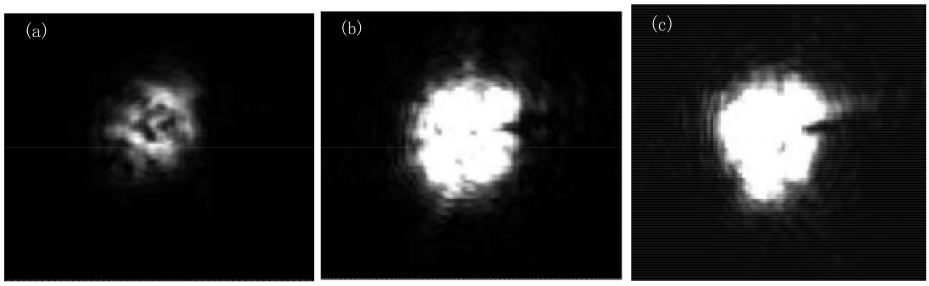

Figure 8. The change in the light pattern in the picture correction experiment. (**a**) Before correction; (**b**) correction without the correction factor, and (**c**) after adding the correction factor correction.

4. Conclusions

The discrepancy in wavefront distortion aberrations within an adaptive optical system represents a systematic error stemming from the disparity in wavefront lengths between the system's signal and beacon lights. By adjusting system parameters and adopting advanced correction algorithms, the impact of turbulence on beam transmission can be

effectively reduced. In our study, theoretical and experimental results show that when the turbulence external scale is greater than 40 m, the speed of wavefront aberration change decreases. Wavelength matching optimization can reduce phase difference, that is, the closer the wavelengths of the beacon light and signal light are, the closer the wavefront aberration is to 0. In numerical simulation, the introduction of correction coefficients in the wavefront correction system increased the SR value from the basic 0.89 to 0.982, by about 11%, and accelerated the convergence speed. In the experiment, the SR value of the spot before and after the implementation of wavefront correction technology jumped from 0.112 to 0.74. After further adding the correction factor, the SR value reached 0.812, an increase of about 10% compared with the initial correction, clearly demonstrating the additional enhancement effect of secondary correction on system accuracy. The further improvement in spot energy and the SR value verifies that this method can effectively improve correction accuracy.

Author Contributions: Conceptualization, M.H. and X.K.; methodology, M.H. and X.K.; software, M.H.; validation, M.H., X.K. and J.L.; formal analysis, M.H.; investigation, M.H.; resources, J.L.; data curation, M.H., X.K. and J.L.; writing—original draft preparation, M.H.; writing—review and editing, M.H. and X.K.; supervision, X.K.; project administration, M.H. All authors have read and agreed to the published version of the manuscript.

Funding: This study was funded by the Key Industrial Innovation Chain Project of Shaanxi Province [grant number 2017ZDCXLGY-06-01] and the General Project of the National Natural Science Foundation of China [grant number 61377080].

Data Availability Statement: The data presented in this study are available on request from the corresponding author. The data are not publicly available due to the limitations of our patent work.

Conflicts of Interest: The authors declare no conflicts of interest.

References

1. Mackey, R.; Dainty, C. Wavefront sensing and adaptive optics in strong turbulence. In Proceedings of the Opto-Ireland 2005: Photonic Engineering, Dublin, Ireland, 4–6 April 2005; Volume 5827, pp. 23–29.
2. Wu, J.L.; Ke, X.Z. Development of adaptive optical correction and polarization control modules for 10-km free-space coherent optical communications. *J. Mod. Opt.* **2019**, *67*, 1–7.
3. Yang, H.Z.; Cai, D.M.; Chen, B. Analysis of adaptive optics techniques without a wave-front sensor and its application in atmospheric laser communications. *Chin. J. Lasers* **2008**, *35*, 680–684. [CrossRef]
4. Dong, B.; Yu, J. Hybrid approach used for extended image-based wavefront sensor-less adaptive optics. *Chin. Opt. Lett.* **2015**, *13*, 21–25. [CrossRef]
5. Jiang, H.L.; Jiang, L.; Song, Y.S.; Meng, L.X.; Fu, Q.; Hu, Y.; Zhang, L.Z.; Yu, X.N. Research of Optical and APT Technology in One-Point to Multi-Point Simultaneous Space Laser Communication System. *Chin. J. Lasers* **2015**, *42*, 150–158.
6. Ma, Y.F. Research on APT Spot Detection Algorithm in Space Optical Communication. *Digit. Technol. Appl.* **2017**, *11*, 115–116.
7. Li, G.; He, Y.L.; Zeng, B. Spot positioning algorithm for laser radar based on triangulation. *Chin. J. Sens. Actuators* **2016**, *29*, 1692–1697.
8. Zhang, J.Z.; Zhang, F.Z.; Li, Y.K.; Wu, Y. Theoretic analysis of expanded beacon's anisoplanatic error. *High Power Laser Part. Beams* **2014**, *26*, 89–95.
9. Li, F.; Jian, R.; Zhong, X.; Ding, X. Study on correcting angle-of-arrival fluctuations of space optical communication with AO. *High Power Laser Part. Beams* **2007**, *6795*, 141–146.
10. Nicholas, D.; Alexander, G.; Christopher, D. Chromatic effects of the atmosphere on astronomical adaptive optics. *Appl. Opt.* **2008**, *47*, 1072–1081.
11. Gorelaya, A.V.; Shubenkova, E.V.; Dmitriev, D.I.; Dmitrieva, A.D.; Kudryashov, A.V.; Lovchiy, I.L.; Shalymov, E.V.; Sheldakova, Y.V.; Tsvetkov, A.D.; Venediktov, D.V.; et al. Investigation of dual-wavelength laser beam propagation along the in-door atmospheric path. In Proceedings of the Conference on Optics in Atmospheric Propagation and Adaptive Systems, Toulouse, France, 22 September 2015.
12. Xu, B.W.; Hu, S.J.; Li, J.; Fan, J.Q.; Tan, Y. Impact of Polarization Chromatic Aberration on Adaptive Optical Systems. *Laser Optoelectron. Prog.* **2020**, *57*, 44–51.
13. Ke, X.Z.; Chen, X.Z. Correcting wavefront distortion of dual-wavelength beams due to atmospheric turbulence with a correction coefficient. *Opt. Photonics J.* **2020**, *10*, 64–77. [CrossRef]
14. Wu, J.L.; Ke, X.Z.; Kang, W.L. Study on the difference of wavefront distortion on beams caused by wavelength-differences in weak turbulence region. *Photonics* **2023**, *10*, 725–739. [CrossRef]

15. Norris, J.R. *Markov Chains*; Cambridge University Press: Cambridge, UK, 1998.
16. Aleksandrovich, K.L.; Rytov, S.M. *Elements of Random Process Theory*; Springer: Berlin/Heidelberg, Germany, 1987.
17. Andrews, L.C.; Phillips, R. *Laser Beam Propagation through Random Media*; SPIE Press: Bellingham, WA, USA, 2005.
18. Zhang, A.C. *Modern Meteorological Observation*; Peking University Press: Beijing, China, 2000.
19. Zhang, Q.; Han, S.; Tang, S.H. Study on functional relationship between transmitted wavefront Zernike coefficients and wavelengths. *Acta Opt. Sin.* **2018**, *38*, 0212002. [CrossRef]
20. Weyrauch, T.; Vorontsov, M.A. Free-space laser communications with adaptive optics: Atmospheric compensation experiments. *J. Opt. Fiber Commun. Rep.* **2004**, *1*, 355–379. [CrossRef]
21. Song, H.; Fraanje, R.; Schitter, G.; Kroese, H.; Vdovin, G.; Verhaegen, M. Model-based aberration correction in a closed-loop wavefront-sensor-less adaptive optics system. *Opt. Express* **2010**, *18*, 24070–24084. [CrossRef] [PubMed]
22. Roddier, N.A. Atmospheric wavefront simulation using Zernike polynomials. *Opt. Eng.* **1990**, *29*, 1174–1180. [CrossRef]
23. Phillips, J.D.; Goda, M.E.; Schmidt, J. Atmospheric turbulence simulation using liquid crystal spatial light modulators. In *Advanced Wavefront Control: Methods, Devices, and Applications III*; SPIE: Bellingham, WA, USA, 2005; pp. 57–67.
24. Shan, X.; Liu, M.; Zhang, N.; Ai, Y. Laboratory simulation of non-Kolmogorov turbulence based on a liquid crystal spatial light modulator. *Opt. Eng.* **2017**, *56*, 026111. [CrossRef]
25. Liu, Y.J.; Hu, L.F.; Cao, Z.L.; Li, D.Y.; Mu, Q.; Lu, X.H.; Xuan, L. Liquid crystal atmosphere turbulence simulator. *Acta Photonica Sin.* **2006**, *35*, 1960–1963.
26. Ai, Y.; Duan, M.Y.; Xu, J.; Shan, X.; Chen, J.; Xiong, Z.; Jiang, R. LC-SLM laser atmospheric transmission turbulence simulation and communication test. *Infrared Laser Eng.* **2015**, *44*, 3103–3109.
27. Liu, C.; Chen, S.; Li, X.; Xian, H. Performance evaluation of adaptive optics for atmospheric coherent laser communications. *Opt. Express* **2014**, *22*, 15554–15563. [CrossRef] [PubMed]